Widely Separate Spectral Sensitivity Quantum Well Infrared Photodetector Using Interband and Intersubband Transitions

Fábio Durante P. Alves, Ricardo Augusto Tavares Santos, Jayr Amorim, Ali Kamel Issmael, Jr., and Gamani Karunasiri, *Member, IEEE*

Abstract—Recent commercial and military infrared sensors have demanded multispectral capabilities, high sensitivity and high selectivity, usually found in quantum well infrared photodetectors (QWIPs). This paper presents the design and characterization of a three-band QWIP capable to detect simultaneously near infrared (NIR), mid-wavelength infrared (MWIR), and long-wavelength infrared (LWIR), using interband and intersubband transitions. Separate readouts provide the flexibility to optimize each band detection by allowing the application of different bias voltages. The quantum well structure was designed using a computational tool developed to solve self-consistently the Schrödinger-Poisson equation with the help of the shooting method. The detector comprises of three different stacks of uncoupled (wide barriers) quantum wells that combine AlGaAs, GaAs, and InGaAs, separated by contact layers, grown by molecular beam epitaxy (MBE) on a GaAs substrate. The spectral responses in all three bands were measured using a standard photocurrent spectroscopy setup with light coupling via a 45° facet. The measured photoresponse showed peaks at 0.84, 5.0, and 8.5 μm wavelengths with approximately 0.8, 0.03, and 0.12 A/W peak responsivities for NIR, MWIR, and LWIR bands, respectively. A good agreement between the measured and simulated figures of merit shows the possibility to improve and tailor the detector for several applications with low computational effort. Finally, this work has demonstrated the possibility of detection of widely separated wavelength bands using interband and intersubband transitions in quantum wells.

Index Terms—Figures of merit, interband transition, intersubband transition, multispectral detection, quantum well infrared photodetector (QWIP), shooting method.

I. INTRODUCTION

RECENT defense applications have demanded photodetectors with high sensitivity, high selectivity, and multispectral capability to detect, identify, and provide high-resolution imaging of a target. These characteristics have been found in QWIPs [1].

The ability of detecting widely separate spectral infrared bands in a single pixel with the flexibility of using separate readouts is demonstrated in this work. To be able to achieve this capability and to assure the feasibility of the device, the following guidelines were pursued [2].

1) Combinations of $GaAs/Al_xGa_{1-x}As/In_xGa_{1-x}As$ on GaAs substrate should be used due to the reliability of material data (properties) found in the literature, lower cost and maturity of crystal growth processes and device fabrication.

2) The peak absorption of the three different bands for temperatures below 77 K should be: the maximum value obtainable for near infrared (NIR) (exploring interband transitions between the ground state of the valence band and the first excited state of the conduction band); as close as possible to 5.0 μm for mid-wavelength infrared (MWIR); and below 9.0 μm for long-wavelength infrared (LWIR).

3) Bound-to-quasi-bound transitions are preferred to minimize the possibility of thermionic transitions, to maximize the oscillator strength and to reduce the amount of bias needed for photocurrent readout.

4) Each band should be detect by a stack of periodic repetitions of a suitable well/barrier configuration. The stacks should be grown onto the substrate in the following sequence: NIR, MWIR, and LWIR. This is to prevent the undesired absorption mechanisms from sequentially blocking the IR bands of passing through their respective detector stacks.

5) The barriers should be wide enough to uncouple the wells in the same stack.

6) The stacks of each band should be limited to 20 repetitions of the basic *barrier/well/barrier* cell due to the complexity to fabricate and to process a large amount of different semiconductor layers.

7) The indium composition in $In_xGa_{1-x}As$ layers as well as the aluminum composition in $Al_xGa_{1-x}As$ layers should be restricted to no more than three different values each in the entire structure to reduce the MBE growing difficulties.

8) The contact layers should be heavily n-doped (about 2.10^{18} cm^{-3}) in order to improve the contact uniformity in big mesas.

9) The cap layer (top) and the contact layer between the MWIR and LWIR quantum well stacks should be thick enough to allow the application of diffraction grating patterns.

Considered the above requirements, the main issue of modeling is to obtain the quantized energy levels inside the quantum

(a)

(b)
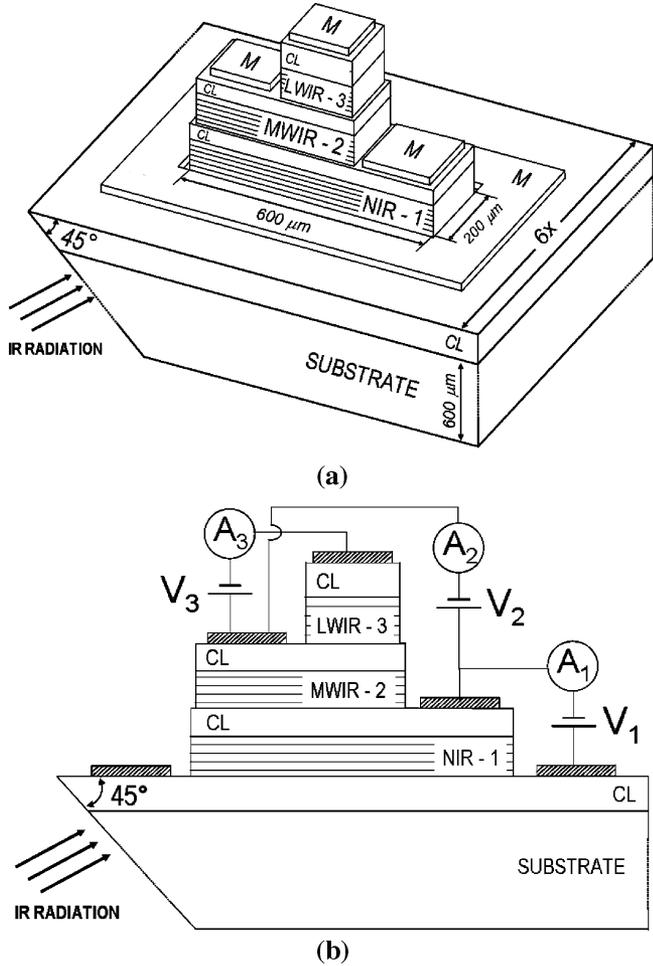
Fig. 1. (a) Schematic 3-D diagram of the multistack device and (b) a vertical cut emphasizing the independent readout configuration.

Fig. 2. Schematic energy-band diagram of the three-band QWIP [4]. The layer thickness are not drawn to scale.

wells, as well as their respective wavefunctions. This is computed self-consistently solving numerically the Schrödinger–Poisson equations. The electron wavefunctions in the structure were obtained using the effective mass approximation for the one-dimensional potential profile along the growth direction. The band nonparabolicity effects were incorporated in the model. For the valence band, the heavy and light hole bands were represented using average negative effective masses, m_{hh} and m_{lh}, respectively. In this case, the well potential is a confining potential for holes and the same model used for electrons in the conduction band becomes applicable. This is done using the shooting method due to its ability to handle arbitrary potential profiles making the design more flexible [3].

Several trials were executed varying the dimensions and the compositions of each band separately resulting in a multilayered device described in the following section.

II. DEVICE DESCRIPTION

The detector consists of three different stacks of quantum wells formed by alloys of GaAs, AlGaAs, and InGaAs, piled on top of each other, separated by n-doped GaAs contact layers, as shown in Fig. 1.

The first well stack is responsible for detecting the NIR due to transitions from ground and excited states (lh and hh) of the

valence band to the first excited state of the conduction band. The well was made asymmetric to allow interband transitions between quantum states with different parity, overcoming the selection rules. The well is not doped to minimize the undesired intersubband transitions.

The second well stack is responsible for mid-infrared detection. It consists basically of symmetric InGaAs quantum wells with AlGaAs barriers, where the intersubband oscillator strength was maximized. Two GaAs layers were placed on the sides of the InGaAs layer to better accommodate the AlGaAs/InGaAs lattice constant mismatch and to reduce the amount of indium in the structure. All three layers of the MWIR quantum well were heavily doped to increase the transition probability.

The stack on the top is responsible for the long-infrared detection. The LWIR absorption occurs in symmetric and shallow AlGaAs/GaAs square wells, where the doping concentration was kept lower than the MWIR wells to reduce the leakage current due to thermionic emission.

According to the selection rules, normal incidence is not capable to cause intersubband transitions between confined levels with consecutive quantum numbers. Therefore, for testing purposes, the light enters into the device normal to a 45° face, as shown in Fig. 1.

The entire structure is comprised of 67 semiconductor layers grown by molecular beam epitaxy (MBE) on a GaAs substrate as follows: a 2×10^{18} cm^{-3} Si doped GaAs (0.7 μm) buffer layer; 20 periods of undoped GaAs (300 Å)/In$_{0.25}$Ga$_{0.75}$As (40 Å)/In$_{0.10}$Ga$_{0.90}$As (43 Å)/ GaAs (300 Å) step quantum wells, a 2×10^{18} cm^{-3} Si doped GaAs (0.5 μm) contact layer; 20 periods of Al$_{0.40}$Ga$_{0.60}$As (300 Å/GaAs (13 Å)/In$_{0.15}$Ga$_{0.85}$As (14 Å)/ GaAs (13 Å)/Al$_{0.40}$Ga$_{0.60}$As (300 Å) quantum wells where the three internal layers were 2×10^{18} cm^{-3} Si doped; a 2×10^{18} cm^{-3} Si doped GaAs (0.5 μm) contact layer; 20 repetitions of Al$_{0.26}$Ga$_{0.74}$As (300 Å)/ GaAs (52 Å)/Al$_{0.26}$Ga$_{0.74}$As (300 Å) quantum wells where the GaAs well was 5×10^{17} cm^{-3} Si doped; and finally, a 2×10^{18} cm^{-3} Si doped GaAs (0.7 μm) cap layer. Fig. 2 shows a schematic band diagram of the sample along with the main transitions, indicated by arrows, responsible for the detection in the three bands of interest.

The wafer was grown by means of contract by IQE, Inc., and the test devices were fabricated by NRC Canada [4]. The theoretical and measured $I-V$ characteristics and responsivities are presented in the following section.

III. FIGURES OF MERIT

A. Dark Current

A biased photodetector with no incident light exhibits dark current. In quantum well devices, three dark current generation mechanisms can be easily identified [5]. First, sequential resonant tunneling can happen causing electrons to "jump" from well to well, through the barriers. This process is independent of temperature and is the dominant source of dark current at lower temperatures. This effect was drastically reduced in the presented structure since large barriers are used to uncouple the wells. The second mechanism is thermally assisted tunneling, which involves thermal excitation and tunneling through the tip of the barrier into the transport states. This process is the dominant source at medium temperatures and can be reduced by placing the final state as far as possible to the initial state. The third mechanism is thermionic emission and it is the dominant source at higher temperatures. To reduce this effect, deeper wells should be considered in combination with less doping.

1) Theoretical Model: Mathematically, it is possible to model the dark current I_D accounting on the influence of thermally assisted tunneling and thermionic emission phenomena through the expression [6]

$$I_D(F) = \frac{q v_{drift} A m_w^*}{\pi \hbar^2 L} \int_{E_1}^{\infty} f^{FD}(E) T(E, F) dE \quad (1)$$

where v_{drift} represents the drift velocity of the electrons in the structure, A represents the photodetector area, m_w^* represents the effective mass inside the well, L is the period of the multiple quantum wells, $f^{FD}(E)$ is the probability of occupation (Fermi–Dirac distribution), and $T(E, V)$ is the transmission function that stands for the probability of tunneling through a single barrier or, simply, tunneling current factor. The tunneling factor in a single barrier is given by [7]

$$T(E, V) = \exp\left(-\frac{4L_b}{3qV}\left(\frac{2m_e^*}{\hbar}\right)^{\frac{1}{2}}\right.$$
$$\left. \times \left[(V_o - E)^{\frac{3}{2}} - (V_o - E - qV)^{\frac{3}{2}}\right]\right) \quad (2)$$

for $E_0 < E < V_o - qV$

$$T(E, V) = \exp\left(-\frac{4L_b}{3qV}\left(\frac{2m_e^*}{\hbar}\right)^{\frac{1}{2}}(V_o - E)^{\frac{3}{2}}\right) \quad (3)$$

for $V_o - qV < E < V_o$ and

$$T(E, V) = 1 \quad (4)$$

for $E > V_o$.

In the previous equations, L_b represents the barrier length, V represents the potential drop across a single barrier (depletion and accumulation effects in the contacts are negligible and any such effect in the MQW are neglected so that V is approximately
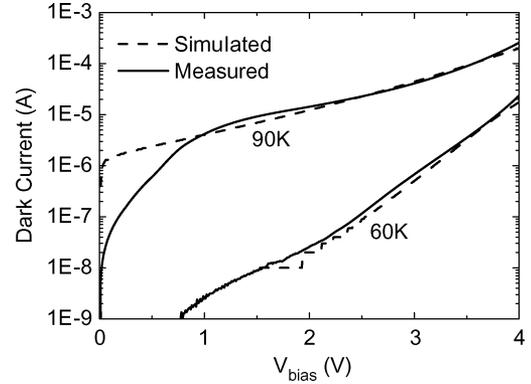
Fig. 3. Comparison between theoretically predict and measured dark current values for LWIR quantum well stacks at temperatures of 90 and 60 K.
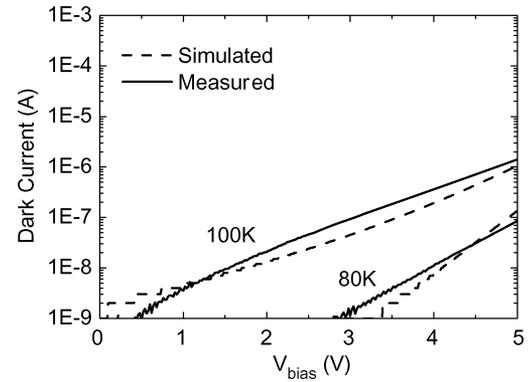
Fig. 4. Comparison between theoretically predicted and measured dark current values for MWIR quantum well stacks at temperatures of 100 and 80 K.

equal to the bias across the detector divided by the number of quantum wells), V_o is the barrier height, and E is the total energy (measured from the bottom of the conduction band).

2) Experimental Setup: The $I-V$ characteristics in the dark were measured using a semiconductor parameter analyzer with the device inside a cold head, where the temperature could be controlled. The device was surrounded by aluminum foil to shield the background infrared radiation. The connections and measurements were done separately, as shown in Fig. 1.

3) Comparison Between Measurements and Simulation: Figs. 3 and 4 present the comparison between theoretically predict and measured dark current values of LWIR and MWIR quantum wells for varying bias voltages and temperatures between 60 and 100 K.

The figures show a good agreement between the theoretical and experimental results. A little discrepancy can be observed for low bias on LWIR dark current, mainly due to the simplification of the mathematical model in computing the quasi-Fermi level and the probability of tunneling. Also, there were neglected important effects such as scattering, the interactions between the three stacks in the structure, and the presence of the GaAs contact layers.

Fig. 5 shows the comparison between theoretically predicted and measured dark current values of NIR quantum wells for varying bias voltages and temperatures from 60 to 90 K with steps of 10 K. The great difference in energy between the initial and final states (see Fig. 2) limits thermally assisted tunneling
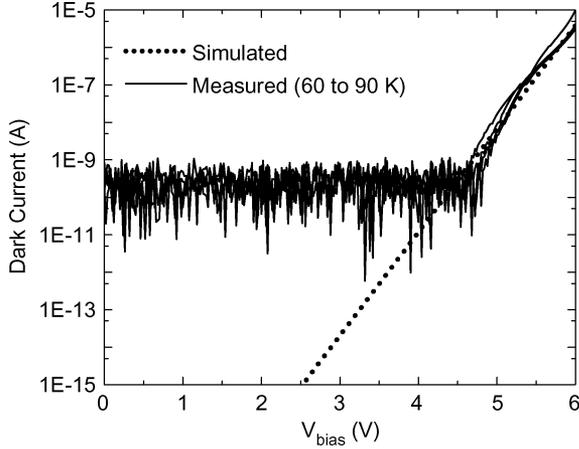
Fig. 5. Comparison between theoretically predicted and measured dark current values for NIR quantum well stacks for temperatures from 60 to 90 K with steps of 10 K.

and the absence of free carriers (no doping) in the conduction band limits the thermionic excitation, keeping the dark current about 10^{-10} A until almost 5 V of applied bias. The clutter seen is most likely due to limitations on the analyzer sensitivity levels. It is possible to observe, in Fig. 5, that the theoretical curve meets the experimental ones for the voltages greater than 5 V. In addition, for those voltages, the curves for different temperatures follow almost the same path, confirming that the temperature dependence of the dark current is very small.

B. Responsivity

The responsivity quantifies the amount of photocurrent ($I_p(F)$) generated per watt of incident radiant photon power (Φ_o). It can be expressed mathematically as [5]

$$R(F) = \frac{I_p(F)}{\Phi_o}. \tag{5}$$

This figure of merit is estimated theoretically and experimentally as follows.

1) Theoretical Model: The photocurrent can be represented by [6]

$$I_P(F) \approx \frac{2q\Phi_o}{\hbar\omega} \alpha L_W \left(\sum_{n=1}^{N} e^{-\frac{nL}{\upsilon(F)\tau}} \right) \tag{6}$$

where α represents the absorption coefficient, $\hbar\omega$ is the photon energy, n is the number of quantum wells, L is the period of the multiple quantum wells, L_W is the width of the well, $\upsilon(F)$ represents the drift velocity under an applied electric field F, and τ is the excited carrier lifetime. Combining (5) and (6), responsivity can be represented by the following expression:

$$R_P(F) \approx \frac{2q}{\hbar\omega} \alpha L_W \left(\sum_{n=1}^{N} e^{-\frac{nL}{\upsilon(F)\tau}} \right). \tag{7}$$

It is important to notice the responsivity dependence on the absorption coefficient (α) and external bias (F). The absorption coefficient is responsible for the shape (spectrum) and the electric field (bias) for the amplitude. Increasing the availability of

carriers (doping concentration), the photocurrent will increase and consequently the responsivity.

The absorption coefficient is the key parameter used in photodetector design. The semiconductor structures are designed to meet the absorption spectra requirements and the absorption coefficient is normally measured after the sample growth, before the device fabrication. In a previous publication [2], detailed models for intersubband and interband bound-to-bound absorption were discussed. The conduction band bound-to-bound intersubband absorption coefficient, α_{CbCb}, is given by the expression [2]

$$\alpha_{CbCb}(\hbar\omega) = \frac{q^2 d}{(m_e^*)^2} \frac{\hbar^3}{\varepsilon_o n_r c(\hbar\omega)} \left| \left\langle \psi_f(z) \left| \frac{\partial}{\partial z} \right| \psi_i(z) \right\rangle \right|^2$$
$$\times \cos^2(\phi) \frac{\Gamma}{(E_f - E_i - \hbar\omega)^2 + (\Gamma/2)^2} \tag{8}$$

where d represents the quantum well doping density, q is the electron charge, c is the velocity of light, ε_o is the vacuum electric permittivity, $\hbar\omega$ is the incident photon energy, $\hbar$ is the Planck constant divided by 2π, m_e^* represents the effective electron mass, ϕ is the angle between the incident flux and the growth axis, $\psi_i(z)$ and $\psi_f(z)$ represent the wavefunctions of initial and final states, respectively, Γ represents the broadening parameter, and E_i and E_f are the ground and excited state energies, respectively. The bound-to-bound interband absorption coefficient α_{VbCb} for the TE mode is given by the expression [2]

$$\alpha_{v_b c_b}^{\mathrm{TE}}(\hbar\omega) = \frac{q^2}{(m_e^*)^2} \frac{m_r^*}{\varepsilon_0 n_r c \hbar(\hbar\omega)} \frac{1}{L} \left((S^{\mathrm{TE}})^2 \frac{m_0}{2} E_p \right)$$
$$\times |\langle \psi_f(z) | \psi_i(z) \rangle|^2 \Theta(\hbar\omega - (E_f - E_i)) \tag{9}$$

where m_r^* represents the reduced mass of the electron-hole system and m_0 is the electron mass. E_p is unanimously accepted in the literature as varying between 17 and 25 meV for most of the III-V binaries. The spin selection rules for the TE mode (S^{TE}) for the light hole (lh) and heavy hole (hh), respectively, are represented by [8]

$$S_{lh}^{\mathrm{TE}} = 1/\sqrt{6}$$
$$S_{hh}^{\mathrm{TE}} = 1/\sqrt{2}. \tag{10}$$

The knowledge of the absorption coefficient for each possible transition in each quantum well allows to employ the expression (7) to describe separately the respective responsivities.

2) Experimental Setup: To permit the estimation of the device responsivity in all three bands, the photocurrent was measured for a range of wavelengths on each band of interest. Fig. 6 shows the schematic diagram of the experimental setup and the estimation sequence.

The IR radiation passes through a monocromator, it is chopped and divided equally in two beams. The first beam passes through a reference detector, with known responsivity, and its photocurrent is measured by a lock-in amplifier. This procedure allows to calculate the electron flux at the detector (Φ_R) and estimate the electron flux going into the test detector (Φ_D), considering the detectors area ratio (A_D/A_R), transmission coefficient of the cold head window (T_W), transmission
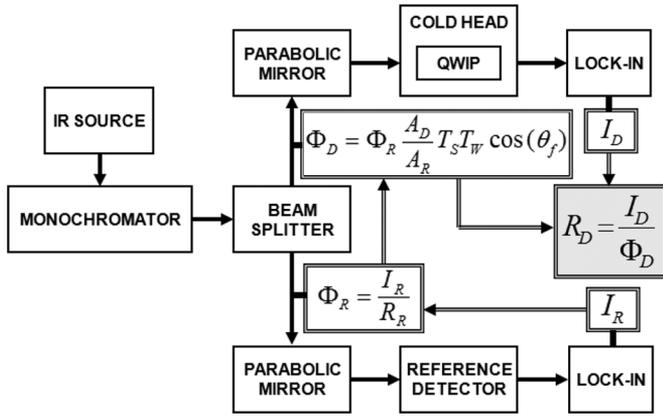
Fig. 6. Schematic diagram of the experimental setup used to perform photocurrent spectroscopy.

TABLE I
PARAMETERS USED IN THE EXPERIMENTAL ESTIMATION
OF THE DEVICE RESPONSIVITY

REFERENCE DETECTOR	
A_R	10 mm²
R_R	1000 V/W (0.8 - 35 μm)
QWIP	
$A_{D\text{-}NIR}$	0.4 mm²
$A_{D\text{-}MWIR}$	0,8 mm²
$A_{D\text{-}LWIR}$	1.2 mm²
T_S	0.68 (NIR - LWIR)
T_W (ZnSe)	0.6 (NIR) - 0.73 (LWIR)
θ_f	45°

coefficient of the substrate (T_S), and the angle of the coupling face $(\cos(\theta_f))$. The second beam goes to the QWIP device placed into a cold head and connected, as shown in Fig. 1(b). The light couples normal to the 45° face. The photocurrent is measured by another lock-in amplifier and the responsivity estimated. In order to remove the background variation effects, measurements were carried with the source shutter closed before and after each scan. The average level of background was subtracted from the overall signal. The key used values are given in Table I.

3) Experimental Results: Figs. 7–9 show the experimental results for the three quantum well stacks in the device. The measurements were performed using the experimental setup described in Fig. 6 with separate bias for each band, as sketched in Fig. 1. All measurements were done at 10 K.

The peak responsivity of LWIR band (Fig. 7) is about 0.12 A/W for a bias of 1.25 V at about 8.4 μm. The curve inflexions around 8.0 μm are due to the filter change. Higher bias voltages do not increase the responsivity, primarily due to saturation of drift velocity of the electrons [5].

The peak responsivity of MWIR band (Fig. 8) is about 0.032 A/W for a bias of 3.5 V at a wavelength slightly greater than 5.0 μm. The spikes seen around 5.4 μm are again
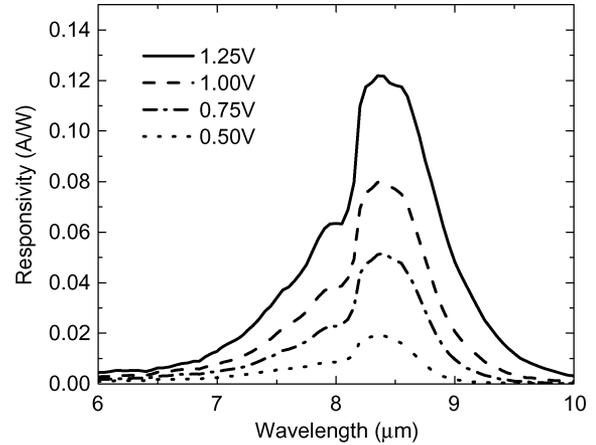
Fig. 7. Responsivity of the LWIR quantum well stack at 10 K, for a set of forward bias voltages.
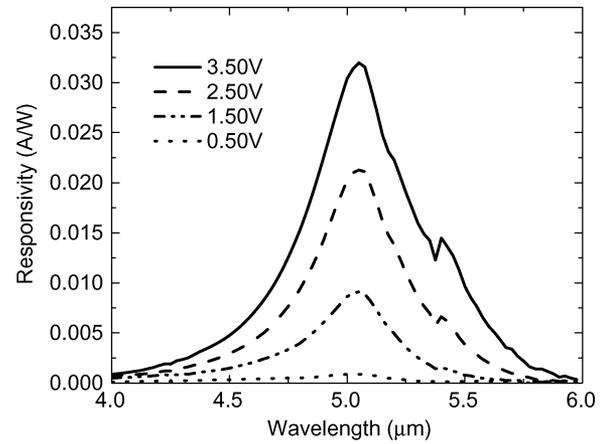
Fig. 8. Responsivity of the MWIR quantum well stack at 10 K, for a set of forward bias voltages.
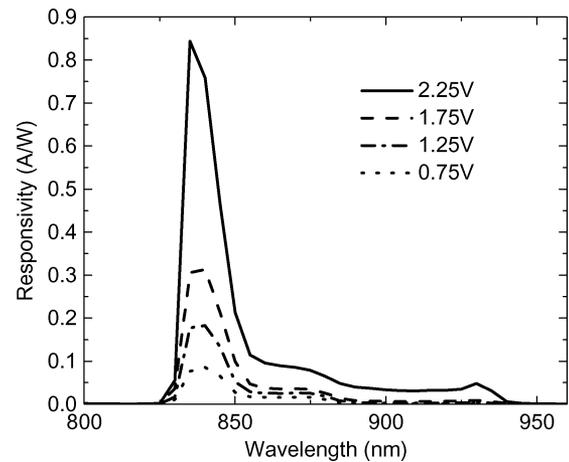
Fig. 9. Responsivity of the NIR quantum well stack at 10 K, for a set of forward bias voltages.

due to the filter change. Even though the doping density in MWIR wells is four times greater than in LWIR wells, the responsivity of the first is much smaller. The MWIR wells are formed by three very thin and strained layers, therefore, due to
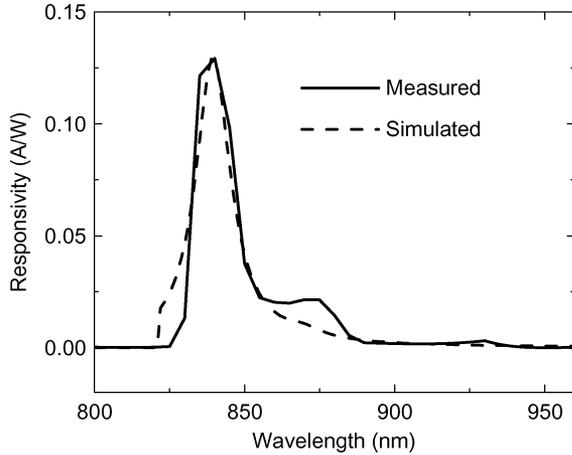
Fig. 10. Comparison between measured and estimated responsivities of the NIR quantum well stack, for an applied bias of 1 V and temperature of 10 K.

Fig. 11. Comparison between measured and estimated responsivities of the MWIR quantum well stack, for an applied bias of 1 V and temperature of 10 K.

Fig. 12. Comparison between measured and estimated responsivities of the LWIR quantum well stack, for an applied bias of 1 V and temperature of 10 K.

limitations in MBE growth, the interfaces are not very sharp, reducing the transition probabilities.

The NIR responsivity curves show transitions from light and heavy holes in three quantized energy levels in valence band to the ground and excited states in conduction band. The peak, around 840 nm, is 0.85 A/W and occurs when the device is under 2.25 V bias. This peak is due to transitions from the valence band first excited state to the conduction band first excited state, the most probable one. The inflexion around 935 nm is due to transitions from the valence band ground state to the conduction band first excited state.

4) Comparison Between Measurements and Simulation: Fig. 10 shows the NIR comparison between theoretical (7) and experimental results for an applied bias of 1 V and temperature of 10 K.

As can be seen in Fig. 10, there is a good agreement between the simulated and the measured curves.

In the NIR stack, the quantum wells are not symmetric resulting nonzero overlap of the wavefunctions of the holes and electrons of all possible transitions (same and different quantum numbers). The transitions between the quantized light and heavy hole levels and the conduction band ground state are also very probable, once the NIR wells are not doped.

Notice that the wavelengths smaller than 820 nm are absorbed by the GaAs substrate. Also, the wavelengths greater than 880 nm are mostly due to the transition to the ground state of the conduction band well. To contribute to the photocurrent, these electrons must tunnel through the barrier, respecting the probability of tunneling expressed in (3). The higher wavelength absorptions are not present due to the very low probability of tunneling of the electrons in the ground state of the conduction band.

Figs. 11 and 12 show the MWIR and LWIR comparisons between theoretical (7) and experimental results for an applied bias of 1 V and temperature of 10 K.

As can be seen in the two previous figures, there is a good agreement between the simulated and the measured curves. The error in wavelength peak is below 2% and it is mainly due to the uncertainties in the band offset parameter of the alloys used to build the potential profile of the structure. The discrepancies in
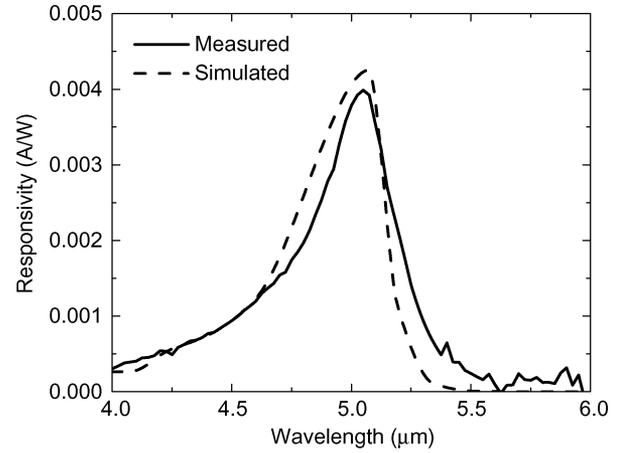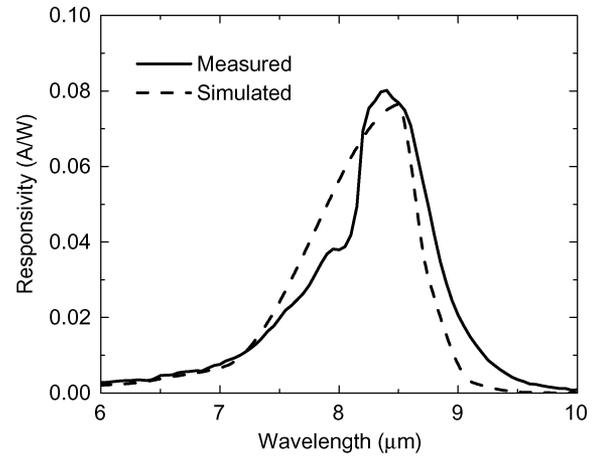
responsivity values are most likely due to the error in estimating the parameters of the (7). In special, excited electron lifetime and drift velocity are difficult to adjust. The area over the curve is bigger in the simulated curves and increases with the external bias. This can be explained as follows. Under bias, the first excited state is pushed out of the well to the continuum states. In this approach, the continuum is discretized and the envelope of the computed absorption peaks is used to determine the spectral behavior of the absorption coefficient of the quantum well. The dicretization resolution is the most probable cause of the observed differences.

IV. FINAL CONSIDERATIONS

A widely separate spectral sensitivity QWIP with the capability to detect simultaneously in NIR, MWIR, and LWIR bands has been demonstrated. The device has the flexibility of separate readouts allowing independent detections in a single pixel. The design is based in three stacks of uncoupled wells (due to large barriers) separated by contact layers. The sample was grown using MBE by means of contract and the test device was fabricated by NRC Canada. Since the test devices have no diffraction grating, the light coupling in all measurements was achieved via

a 45° face polished on one side of the device. The photocurrent model of [7] was adapted to estimate the $I - V$ characteristics of the three bands. The responsivity of each band quantum wells were computed basically using the absorption coefficient developed in previous work [2] and parameters such as excited electron lifetime and drift velocity, obtained from the literature [7]. The Schrödinger equations in the structure were solved with the help of the shooting method. The results show good agreement between the theoretical predictions and the experimental results indicating the method can be used to design detectors that use interband and intersubband transitions, without need of heavy computation. This device shows great flexibility and potential to be improved and adapted to meet the requirements of several modern applications.

REFERENCES

[1] A. Rogalki, "Third-generation infrared photon detectors," *Opt. Eng.*, vol. 42, no. 12, pp. 3498–3516, 2003.

[2] F. D. P. Alves, "Design and analisys of a multicolor QWIP," M.S. thesis, Naval Postgraduate School, Monterey, CA, 2005.

[3] P. Harrison, *Quantum Wells, Wires and Dots: Theoretical and Computational Physics*. New York: Wiley, 2001, pp. 23–30.

[4] F. D. P. Alves, "NIR, MWIR and LWIR quantum well infrared photodetector using interband and intersubband transitions," *Infrared Phys. Technol.*, vol. 50, pp. 182–186, 2007.

[5] B. F. Levine, "Quantum well infrared photodetectors," *J. Appl. Phys.*, vol. 74, no. 8, pp. 1–81, 1993.

[6] R. P. Karunasiri, J. S. Park, and K. L. Wang, "Progress of SiGe/Si quantum wells for infrared detection," in *Thin Films*. San Diego, CA: Academic, 1995, vol. 21, pp. 77–112.

[7] S. R. Andrews and B. A. Miller, "Experimental and theoretical studies of the performance of quantum well infrared detectors," *J. Appl. Phys.*, vol. 70, no. 2, pp. 993–1004, 1991.

[8] E. Rosencher and B. Vinter, *Optoelectronics*. London, U.K.: Cambridge Univ. Press, 2002, pp. 344–350.

Fábio Durante P. Alves was born in Ribeirao Preto-SP, Brazil, on February 10, 1965. He graduated with a Degree in electrical engineering and received the Master of Science Program degree in the realm of signal processing of photonic sensors from the Instituto Tecnologico de Aeronáutica (ITA), Sao Jose dos Campos, SP, Brazil, in 1997 and 1998, respectively. He earned the Electrical Engineer degree from the Naval Postgraduate School (NPS), Monterey, CA, in 2005. He is currently working towards the Ph.D. degree at the Physics Department, ITA.

He has been working in research and development of quantum well infrared photodetectors. He is an Assistant Professor in the Electronic Engineering Department, ITA.

Ricardo Augusto Tavares Santos was born in Rio de Janeiro, Brazil, on April 6, 1971. He completed the Master of Science Program degree from the Instituto Tecnológico de Aeronáutica (ITA), São José dos Campos, SP, Brazil, in 2004. He is currently working towards the Ph.D. degree at the Electronic Engineering Department, ITA

He has been working in research and development of quantum well infrared photodetectors.

Jayr Amorim was born in Rio de Janeiro-RJ, Brazil, on December 12, 1959. He graduated with a Degree in electrical engineering from the Faculdade de Engenharia, Sao Jose dos Campos, SP, Brazil, in 1987, the M.Sc. degree in the realm of electrical discharge from the Instituto Tecnologico de Aeronautica (ITA), Sao Jose dos Campos, SP, Brazil, in 1989, and the Dr. en Sc. degree in physics from the University of Paris, Orsay, in 1994.

He is a Professor at the Physics Department, ITA and Coordinator of Researches in Atomic and Molecular Physics.

Ali Kamel Issmael, Jr. was born in Rio de Janeiro, Brazil, on August 24, 1974. He graduated with a Degree in electrical engineering from Rio de Janeiro State University (UERJ), Rio de Janeiro, Brazil, in 1999.

He worked in the development of quantum well infrared photodetectors during his technical specialization course at the Instituto Tecnológico de Aeronáutica in 2006.

Gamani Karunasiri (M'90) received the B.S. degree in physics from the University of Colombo, Sri Lanka, in 1979, and the M.S. and Ph.D. degrees in physics from the University of Pittsburgh, Pittsburgh, PA, in 1981 and 1984, respectively.

He is a Professor of Physics at the Naval Postgraduate School, Monterey, CA, since 2000. He was a Research Scientist at Microtronics Associates (1985–1986) and was an Assistant Research Engineer at the University of California, Los Angeles (1987–1993). From 1994 to 2000, he was a faculty member of the Department of Electrical Engineering, National University of Singapore, where he developed a microbolometer-based infrared camera. He is the author of over 85 journal publications and holds three patents. His current research interests are in quantum well infrared detectors, MEMS-based directional sound sensors, and THz imaging using quantum cascade laser (QCL) and microbolometer camera.